Suppression of material transfer at contacting surfaces: the effect of adsorbates on Al/TiN and Cu/diamond interfaces from first-principles calculations

OPEN ACCESS
IOP Publishing
Journal of Physics: Condensed Matter
J. Phys.: Condens. Matter **30** (2018) 105001 (11pp)
https://doi.org/10.1088/1361-648X/aaac91

Suppression of material transfer at contacting surfaces: the effect of adsorbates on Al/TiN and Cu/diamond interfaces from first-principles calculations

Gregor Feldbauer[1,2,3], Michael Wolloch[2,3,4], Pedro O Bedolla[2,3], Josef Redinger[2], András Vernes[2,3] and Peter Mohn[2]

[1] Institute of Advanced Ceramics, Hamburg University of Technology, Denickestraße 15, 21073 Hamburg, Germany
[2] Institute of Applied Physics, Vienna University of Technology, Wiedner Hauptstraße 8-10/134, 1040 Vienna, Austria
[3] Austrian Center of Competence for Tribology, AC2T research GmbH, Viktor-Kaplan-Straße 2/C, 2700 Wiener Neustadt, Austria
[4] Department of Physics, Informatics and Mathematics, University of Modena and Reggio Emilia, Via Campi 213/A, 41125 Modena, Italy

E-mail: gregor.feldbauer@tuhh.de

Received 10 November 2017, revised 19 January 2018
Accepted for publication 2 February 2018
Published 16 February 2018

Abstract

The effect of monolayers of oxygen (O) and hydrogen (H) on the possibility of material transfer at aluminium/titanium nitride (Al/TiN) and copper/diamond (Cu/C_{dia}) interfaces, respectively, were investigated within the framework of density functional theory (DFT). To this end the approach, contact, and subsequent separation of two atomically flat surfaces consisting of the aforementioned pairs of materials were simulated. These calculations were performed for the clean as well as oxygenated and hydrogenated Al and C_{dia} surfaces, respectively. Various contact configurations were considered by studying several lateral arrangements of the involved surfaces at the interface. Material transfer is typically possible at interfaces between the investigated clean surfaces; however, the addition of O to the Al and H to the C_{dia} surfaces was found to hinder material transfer. This passivation occurs because of a significant reduction of the adhesion energy at the examined interfaces, which can be explained by the distinct bonding situations.

Keywords: DFT, heterointerfaces, nanotribology, material transfer, adhesion, passivation, electronic structure

S Supplementary material for this article is available online

(Some figures may appear in colour only in the online journal)

1. Introduction

Understanding atomistic phenomena at contacting surfaces is fundamental to the improvement of modern applications, ranging from experimental methods like atomic force microscopy (AFM) [1] to nanotechnologies such as nano-/micro-electro-mechanical-systems (NEMS/MEMS) [2, 3]. Particularly, nanotribological processes, like nanoscale wear [4–8], are not yet understood comprehensively because of their high complexity [9].

Heterointerfaces between metals and counterparts like ceramics [10] or diamond [11] combine benefits of involved material classes, such as high thermal stability, degradation resistance, and interesting mechanical properties [12, 13]. With applications ranging from protective coatings to communication devices and (nano)electronics [14, 15] such interfaces have proved their technological significance. Two distinct, technologically highly relevant pairings each consisting of a hard and a soft material are investigated in this paper, namely the metal-ceramic Al/TiN interface and the metal-insulator Cu/diamond (C_{dia}) interface.

In reality, however, surfaces are usually not pristine. For example, when aluminum is exposed to air a thin oxide film is formed at the Al surface. This passivation prevents further oxidation and results in an excellent corrosion resistance of the material [16]. The typical thickness of such a film is up to 50 nm. As a first approximation on the route towards such exceedingly complex interfaces, the effect of a monolayer of oxygen covering Al surfaces will be discussed in this work. The adsorption of oxygen atoms at an Al surface also constitutes the initial step during the formation of surface oxides. For C_{dia} it is important to consider the effect of hydrogen atoms, because they play a crucial role in the chemical vapour deposition (CVD) growth of diamond and they passivate dangling bonds at diamond surfaces [13, 15]. Thus, the influence of a monolayer of hydrogen at diamond surfaces is investigated here.

The electronic and atomic structure of the studied interfaces are investigated via density functional theory (DFT) calculations allowing, e.g. to determine adhesion energies. DFT calculations, which have been increasingly used in nanotribology during the last decade, see e.g. [17–26], give very reliable results for complex systems and surfaces because of an accurate quantum-mechanical description [27–29]. On the other hand, such calculations are currently limited in size to typically a few hundred atoms because of computational challenges. Thus, DFT should be seen as an extension to and not as a replacement for the more common computational tools in tribology, particularly classical molecular dynamics (MD) simulations [30–39]. DFT results, such as potential-energy curves, can be utilized as a starting point for a multi-scale approach in which data is handed over to, e.g. large-scale classical MD simulations [40, 41]. In the last years also quantum-classical embedding techniques have been developed and improved allowing to treat crucial parts of a system with high accuracy methods such as DFT, while most of the system is evaluated using less expensive methods [42–44]. Such joint approaches combined with advances in software tools and the continuously increasing available computer power promise the feasibility to study even larger and more realistic systems in the near future.

Investigations on Al/TiN interfaces have been conducted by various research groups using experimental [10, 45–48] as well as theoretical [25, 49–57] methods. The role of interfacial species at Al/TiN interfaces is, however, less studied. Liu *et al* [58] and Zhang *et al* [52] investigated the effects of hydrogen and Zn as well as Mg, respectively, on Al/TiN interfaces. Both computational studies concluded that the interfacial adhesion is reduced by the additional species at the interface. Here, the emphasis lies on the role of oxygen, since aluminium is usually covered by an oxide layer under ambient conditions [16]. Further information on oxide layers on aluminium surfaces can be found, e.g. in [59, 60]. As a first step towards a more detailed description of Al/TiN interfaces, the Al slab is terminated by one layer of oxygen in the current work, which focuses on a possible material transfer and its *ab initio* simulation. Material transfer is here defined as the detachment of atoms or atomic layers from one body and the reattachment to the counterbody during the course of one loading cycle. In this context one loading cycle describes the approach, contact and subsequent separation of two initially separated bodies.

Insights on copper/diamond interfaces with and without interfacial species have been presented by various researchers [11, 13, 61–67]. Cu/C_{dia} will be used as an abbreviation in the following. For Cu/C_{dia} interfaces, Guo *et al* [11] studied the fracture behaviour by comparing the work of separation and the work of decohesion. The structure and work of separation for such interfaces including H terminated diamond was examined computationally by Wang and Smith [13]. They found a strong decrease in the adhesion energy and thus the work of separation of Cu/C_{dia} interfaces upon the introduction of interfacial hydrogen, but they did not investigate material transfer explicitly. Their results are in agreement with experiments performed by Pepper [66] on the frictional properties of these interfaces. Furthermore, in a recent study involving MD simulations of nanoscratching Zhu *et al* [67] observed that the minimum depth of material transfer at Cu surfaces can be as thin as only one atomic layer of Cu depending on the machining conditions. In this work, as for the Al/TiN interfaces, the emphasis is put on material transfer and its *ab initio* simulation.

2. Computational details

2.1. Density functional theory calculations

DFT calculations were performed of the approach and subsequent separation of two slabs forming either Al/TiN interfaces or Cu/C_{dia} interfaces including interfacial species. The focus of this paper is put on Al/TiN interfaces, while results on contacting Cu and diamond slabs are given for comparison, as a validation of the method, and a more general view of the subject. All results were calculated using the Vienna *Ab initio* Simulation Package (VASP) [68–71]. Periodic boundary conditions, a plane-wave basis set, and projector augmented-wave (PAW) pseudopotentials [72, 73] were employed. In general,

the exchange and correlation (XC) functional was described by the generalized gradient approximation (GGA) in the Perdew, Burke, and Ernzerhof (PBE) parametrization [74]. Additionally, the local-density approximation (LDA) [75] and the van der Waals (vdW) density functional (DF) optB86b [76, 77] were used for comparison and to check the consistency of the results. While GGAs often underestimate binding and adhesion energies [78], LDA usually overestimates these quantities [79]. Further examples and occasional deviations from this trend are presented in [80]. Therein, it is observed that LDA and GGA results on material properties often give a lower and upper bound for corresponding experimental data. Some trends exist for specific properties, e.g. LDA often performs better for surface energies, while PBE gives usually better results for elastic properties and cohesive energies [81, 82]. No functional is, however, considered to be generally superior to the other ones. The 'opt' vdW-DFs approximate vdW interactions via a nonlocal correlation term and yield good accuracy for diverse materials, e.g. see [23, 83–87]. In an earlier publication [25] it was shown that vdW interactions have no influence on material transfer for Al/TiN interfaces between clean surfaces; however, here this is checked again for weakly bound interfaces.

Accurate total energies are guaranteed by a careful choice of the computational parameters which were extensively tested and presented in an earlier publication [25]. Just the main points are given here, while the details from [25] are repeated in the supplemental material (stacks.iop.org/JPhysCM/30/105001/mmedia). A Γ-centred $15 \times 15 \times 1$ Monkhorst–Pack k-point mesh [88] was used and the energy cutoff for the plane-wave basis was set to 800 eV. For metallic Al/TiN, atomic relaxations were performed employing the method of Methfessel and Paxton [89] to first-order with a smearing of 0.11 eV, while Gaussian smearing of 0.05 eV was chosen for Cu/C_{dia}.

2.2. Simulation model

The simulation model is described here for the case of an Al/TiN interface, using the methodology presented by the authors in an earlier publication [25]. The main points are repeated here and certain novelties in the methods are added, but the reader is referred to [25] for a more detailed account. The same methodology is applied for Cu/C_{dia} interfaces.

The Al/TiN model system was constructed from a fcc (1 1 1) Al slab at the bottom and a rock salt (1 1 1) TiN slab above (see figure 1). The 'interface distance' is measured from the top layer of the lower slab to the bottom layer of the upper slab, regardless of termination, while 'slab height' refers to the vertical distance between the bottom Al and top TiN layers. The interface distance and the slab height describe the gap between the slabs and this gap plus the heights of the two slabs, respectively. To investigate the effect of oxygenation, an Al slab was terminated by oxygen at the interface (see figure 1). The 1×1 surface cells used here represent infinitely extended surfaces because of the periodic boundary conditions. The TiN slab consisted of a minimum of six Ti and six N layers, while the Al slab consisted of seven layers. These

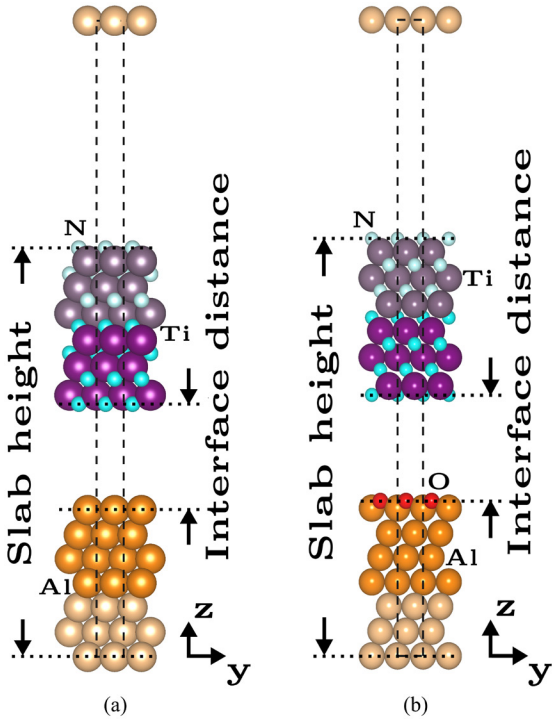

Figure 1. Side view of two (1 1 1) Al/TiN interfaces (TiN: N terminated). The Al slab is pristine in (a) and oxygenated in (b). The simulation interface cell is indicated by the dashed black lines. Orange, red, cyan, and purple identify Al, O, N, and Ti atoms, respectively. During relaxations the pale colors indicate atoms that were kept frozen, while the strong colors mark atoms that were allowed to relax. (a) Al/TiN (hcp) and (b) Al–O/TiN (top).

geometric parameters are consistent with previous investigations [25, 49, 51, 54, 90].

The (1 1 1) surface of a TiN slab is either terminated by Ti or N depending on the chemical potential of nitrogen. In an earlier publication [25] it was shown that both cases are found in reasonable nitrogen concentration ranges in agreement with literature [49, 91]. In this work the main focus is put on N terminated slabs, since this termination is favorable at small deviations of the nitrogen chemical potential from its molecular reference, i.e. at ambient conditions. Over a wide range of the nitrogen chemical potential the (0 0 1) TiN surface is actually the most stable orientation; however, Al/TiN interfaces between (0 0 1) slabs do not show any material transfer [25]. Interfaces between (1 1 1) surfaces show a similar stability at certain values of the chemical potential and allow for material transfer at least between pristine surfaces. Thus, results for (1 1 1) interfaces are presented in this work.

For the Al/TiN interface simulation cells, an intermediate lattice parameter of 4.144 Å was selected for the lateral *xy* lattice vectors yielding an equalized relative error of about 2.6% for both materials. The consequences of such distortions were investigated in detail in an earlier publication [25], where no influence of the chosen lattice parameter on the occurrence of material transfer was observed. In that paper also the simplifications made in this approach are discussed with respect to real systems. Assuming a pseudomorphic interface, for the *z* direction the material-specific values for the layer distances were used.

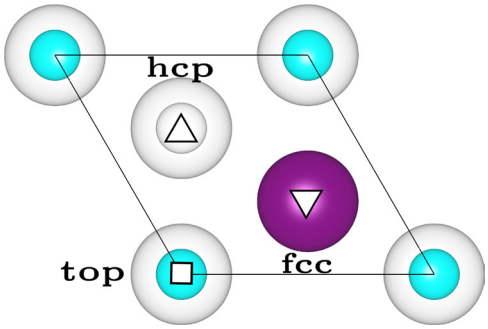

Figure 2. Top view a 1×1 surface cell of a N-terminated (1 1 1) TiN surface. Filled circles indicate atoms in the top surface layer for each species (Ti and N are given by large purple and small cyan circles, respectively), while empty circles label atoms below the top surface layer. To obtain a Ti-terminated (1 1 1) TiN surface the Ti and N atoms of the shown N-terminated surface have to be exchanged. High-symmetry points (top, hcp, fcc) are highlighted.

The simulation of the approach and separation of the slabs also follows the method presented and described in [25]. For the convenience of the reader the main points are repeated here. The variation of the gap between the two slabs was simulated by moving the upper slab in discrete steps along the z direction and allowing for electronic and atomic relaxations after each step. Figure 1 shows the 'frozen' atoms and the 'free' atoms during atomic relaxations for the N-terminated case. In general, defining the interface as the center the outer three layers of each species are kept frozen, while the more central layers are allowed to fully relax. For the approach and separation step sizes of 0.2 Å and 0.1 Å, respectively, were used. For the observation of material transfer the separation is more critical; therefore, a smaller step size was used, which allows for higher accuracy but increases computational costs. This quasi-static method is used because real systems are considered to behave adiabatically during the investigated processes [25]. The approach and separation of the slabs were initiated from 'equilibrium' structures, i.e. separately relaxed slabs and the structure with the lowest energy determined during the approach, respectively. For a more realistic separation process only the topmost, frozen TiN layers were moved in discrete steps in the positive z direction. This procedure was employed to guarantee that a separation of the slabs at the initial interface was not promoted by the enforced step-wise motion. Because of the dimensions of the simulation cell, the transfer of entire atomic layers is investigated. This is seen as a limiting scenario of more realistic rough interfaces where the transfer of clusters or flakes of atoms is likely. A more detailed discussion on size, strain, and surface effects can be found in an earlier publication [25].

The effects of different local environments at the interface were investigated by studying several lateral alignments of the slabs with respect to each other. These different configurations represent limiting scenarios for more complex realistic interfaces [25]. The definitions of the alignments are shown in figure 2 by marking the high-symmetry points on the N-terminated (1 1 1) TiN surface where the next Al or O atom can be placed. The alignments are named according to the stacking of the bottom TiN layer with respect to the Al slab, the position of interfacial species is not taken into account in this naming convention. The different configurations are compared via the interaction energy $E_{\mathrm{I}}(z)$, which is defined as the difference of the total energy of the interacting slabs $E_{(\mathrm{Al/TiN})}(z)$ at slab height z and the reference energies of the two independent slabs, $E_{(\mathrm{Al})}$ and $E_{(\mathrm{TiN})}$,

$$E_{\mathrm{I}}(z) = E_{(\mathrm{Al/TiN})}(z) - E_{(\mathrm{Al})} - E_{(\mathrm{TiN})}. \quad (1)$$

Table 1. Calculated energy costs to remove the top two Al layers, with and without an additional oxygen layer, from an oxygenated and a pristine [25] Al slab, respectively, using PBE, LDA, and optB86b-vdW. The removal energies are given in eV per 1×1 surface cell.

	PBE	LDA	optB86b
Pristine Al	0.803	0.975	0.960
Oxygenated Al	0.804	0.988	0.966

3. Results and discussion

3.1. Oxygen adsorption at an Al slab

The fcc adsorption site is favoured by a single oxygen atom on a 1×1 (1 1 1) Al surface cell. The oxygen is strongly bound to the Al surface exhibiting a rather small binding distance of about 0.7 Å with an adsorption energy of about −4.7 eV with respect to molecular, gas-phase oxygen [59]. The hcp site is slightly less favourable by about 0.2 eV, while the interaction on the top site is much weaker and not favorable considering molecular oxygen as the reference. Additionally, the placement of two O atoms on each 1×1 Al surface cell was tested. The two atoms were located initially above the fcc and hcp sites of the Al surface. During a subsequent relaxation the fcc O atom moved beneath the top Al layer, while the hcp O atom stayed above the Al surface. The distance between the top O–Al compound and the remaining O terminated Al slab grew to about 4.2 Å. This large distance combined with a very weak adhesion (−10 meV) of this compound on the surface shows that the termination with one O atom per surface cell is preferential on a 1×1 Al surface cell. The possibility of an Al_2O_3-like surface oxide [60] is not considered here.

Since material transfer at interfaces is of interest, the energy necessary to remove layers from a material is an important quantity. For this work, the additional question arises whether this removal energy is affected by an oxygen layer. The removal of the layers was simulated by placing them at a large distance from the remaining slab. The distance was chosen large enough to suppress interactions between the slab and layers. Results for pristine Al slab including the effect of compressive and tensile stress were presented in an earlier publication [25]. Here, only the values necessary for comparison are repeated in table 1. Typically, it is energetically unfavourable to remove just one Al layer compared to at least two layers. Moreover, the removal energies are not changing significantly for two or more layers; therefore, the removal of two Al layers is used as a reference here. As mentioned above, oxygen is strongly bound to the Al slab. Thus, it is unlikely that only the

oxygen is removed and so the more plausible case of and the removal of the oxygen layer together with Al layers is investigated here. The data in table 1 shows that an oxygen layer hardly influences the removal energies which indicates that the bond breaking between the Al layers is the determining factor. Nevertheless, oxygen may still passivate a surface by suppressing interactions, i.e. weakening the interfacial adhesion, across an interface with another material such as TiN.

3.2. Lateral alignments at the Al/TiN interface

Effects of different lateral configurations of the slabs at the interface (see figure 2) were studied with and without oxygen at the interface. These investigations showed the strong relative dependence of equilibrium properties such as adhesion energies on the chosen alignment. The adhesion energies are energetically one order of magnitude larger for the Al/TiN interface than for the oxygenated contact. The calculated interaction energies (equation (1)), of relaxed Al/TiN and Al–O/TiN interfaces are displayed in figure 3 for slab heights around the energy minima. For each alignment, these minima are equivalent to the adhesion energies. For the pristine Al slab, in general, the top Al atoms prefer the proximity of N atoms over Ti atoms. More details on interfaces and the bonding situations between pristine Al and TiN slabs can be found in [25]. For the oxygenated Al slab in contact with a TiN slab the adhesion energies are strongly reduced compared to the pristine case. The absolute difference between different alignments is, therefore, also rather small. The main focus of this work is on the possibility of material transfer at such interfaces. It has been observed experimentally [47, 48] as well as in simulations [25] that metal-ceramic interfaces with weak and strong interfacial adhesion break upon stress at the interface and in bulk areas, respectively. This trend is confirmed by the present calculations.

As discussed in more detail in [25], material transfer between the slabs should only occur from an energetical point of view if the energy cost to remove layers is compensated for by the energy gain due to adhesion. This argument is sketched in figure 3 by including a horizontal line at the negative value of the Al or Al–O removal energy. We find that the pristine and oxygenated surfaces studied here exhibit entirely different behaviour. In the non-oxygenated case all configurations should lead to the transfer of at least one Al layer, while, the presence of oxygen at the interface should suppress material transfer for all investigated cases.

For a more comprehensive understanding of the differences between oxygenated and non-oxygenated Al surfaces at Al/TiN interfaces, layer-resolved densities of states (DOSs) and differences in charge densities are investigated. Layer-resolved DOSs of the valence electrons are shown in figures 4 and 5 for Al/TiN and Al–O/TiN interfaces, respectively. In both figures 'interface (surface) layers' correspond to the first layers of Al, Ti, and N immediately at the interface (surface). DOSs for the 'sub-interface (sub-surface) layers', which indicate the next layers of Al, Ti, and N moving deeper into both materials, are given in the supplemental material. Additionally, orbital-resolved DOSs for the surface and

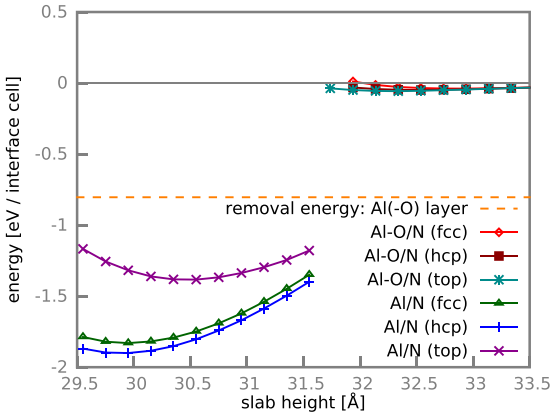

Figure 3. Calculated PBE interaction energies of the relaxed Al/TiN and Al–O/TiN interfaces for the (1 1 1) N-terminated surface orientations. Various lateral alignments of the two slabs are considered, see figure 2. The horizontal, dashed orange line gives the energy costs to remove at least one Al layer from an (1 1 1) Al slab. The Al–O removal energy from an oxygenated Al slab is almost equivalent.

interface layers are presented in the supplemental material. For the non-oxygenated Al surface the DOSs of the isolated surfaces and the interface display distinct features, particularly, for the surface and interface layers, see figure 4. The N sp as well as the Ti sd states are broadened and shifted to lower energies, while the Al sp states show concentrations around −8 eV mainly for the s states as well as −6 eV mainly for the p states and less pronounced around −16 eV resulting in common peaks with N p states and Ti d states. These changes of the interfacial DOSs indicate a hybridization of Al and N states and explain the strong adhesion because of covalent interactions. The common peaks of Al and Ti states arise because of strong interactions between N and both other atomic species and not due to direct Al–Ti interactions which is in agreement with results for (0 1 1) Al/TiN interfaces [25].

For an oxygenated Al surface the consequences of a contact with a TiN surface are quite different, see figure 5. First, the strong interaction between the Al surface and the O monolayer is clearly visible. For comparison, the DOSs of the sub-surface layers can be seen in the supplemental material. The surface layer DOS shows common peaks of the Al sp and O states around −21 eV for O s states as well as −8 eV and −6 eV for O p states explaining the strong bond between Al and O. Furthermore, the decrease of Al states beyond the Fermi energy upon oxygen adsorption indicates that O electrons populate those states. This reduction of available Al states decreases its reactivity. Contrary to the Al/TiN contact, the DOSs of the isolated and interacting Al–O slabs and TiN slabs are almost equivalent and exhibit no indication for a pronounced interaction between an Al–O slab and a TiN slab. This finding agrees well with the very low adhesion energies reported for these interfaces above. The interfacial alignments used here to obtain the DOSs result in the largest adhesion energies for the respective systems. The same trends as described above can be also seen for alignments yielding the weaker interfaces. The corresponding DOSs for these cases are presented in the supplemental material.

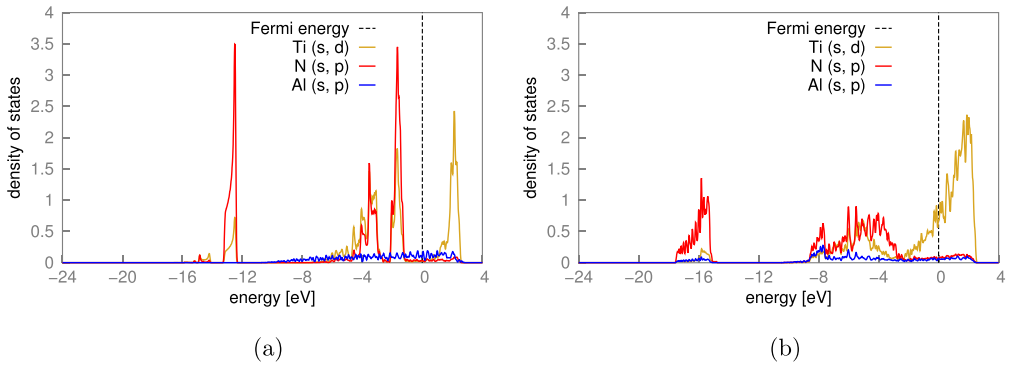

Figure 4. Layer-resolved DOSs from PBE calculations for the surface/interface layers of the isolated Al and TiN slabs in (a) as well as of the Al/TiN (1 1 1) interface for the Al/N (hcp) alignment in (b). The Fermi energy is set to 0 eV. (a) Al and TiN: surface layers and (b) Al/N (hcp): interface layers.

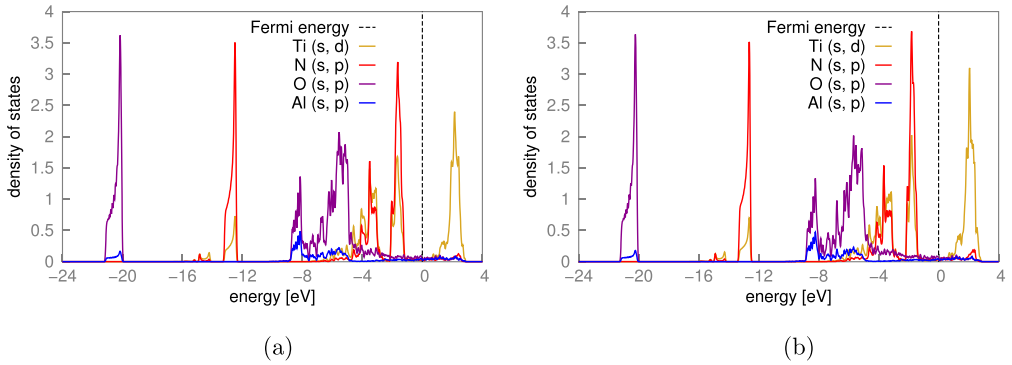

Figure 5. Layer-resolved DOSs from PBE calculations for the surface/interface layers of the isolated Al–O and TiN slabs in (a) as well as of the Al–O/TiN (1 1 1) interface for the Al–O/N (top) alignments in (b). The Fermi energy is set to 0 eV. (a) Al–O and TiN: surface layers and (b) Al–O/N (top): interface layers.

To support the DOS arguments, charge densities at the interfaces are examined. Particularly, the differences of charge densities ρ_{diff} between the isolated, independent Al and TiN slabs and the Al/TiN interface are used, which are calculated via

$$\rho_{\text{diff}} = \rho_{\text{Al/TiN}} - (\rho_{\text{Al}} + \rho_{\text{TiN}}) \quad , \tag{2}$$

where $\rho_{\text{Al/TiN}}$ is the charge density of the interface and ρ_{Al} as well as ρ_{TiN} are the charge densities of the isolated slabs. Such charge-density differences are visualized as isosurfaces in figure 6 for Al/TiN and Al–O/TiN interfaces. For the non-oxygenated Al surface a significant charge accumulation at an Al/TiN interface is found near the interfacial N atoms pointing towards the neighbouring Al atoms (see figure 6). This indicates covalent contributions to the interfacial bonding. Furthermore, a charge buildup at the interfacial Ti atoms is observed with contributions parallel to and towards the interface. For clarity, the charge-density differences are integrated in the two dimensions parallel to the interface. The values are normalized to the interfacial cross-section. The results $\rho_{\text{diff}}(z)$ for these integrated charge-density differences along the axis perpendicular to the interface, i.e. in the [1 1 1] direction, are shown in figure 6 for a limited region around the interfaces. Such charge-density profiles were used, e.g. to successfully analyse changes in adhesion and corrugation at interfaces [92]. Both representations in figure 6 indicate a much weaker interaction for oxygenated interfaces. For the oxygenated Al surface the charge-density differences at an Al–O/TiN interface are smaller by about a factor of five; therefore almost no effect is visible in figure 6. Since Al–O and TiN slabs are used as a reference, the effect of oxygen on the charge distribution in an Al slab is not given. Corroborating the findings from the DOS analysis these charge-density results also suggests a much weaker bond because of the additional oxygen layer.

3.3. Approach and separation of Al and TiN slabs

Material transfer at interfaces can be studied by ‘slowly’, in the sense of using small discrete steps, approaching and subsequently separating the slabs. Figure 7 displays the energetical results of such loops for different Al/TiN and Al–O/TiN configurations; the most important information is presented in table 2. The ‘approach—static’ curve in figure 7 represents a static interaction-energy curve. This data was obtained from calculations where all atoms were kept frozen for each selected interface distance. For large interface distances, differences between static calculations and those including atomic relaxations are small because of the lack of strong interactions between the slabs. For ever-shorter distances, however, the effect of interactions increases, and the relaxed-energy data deviate from the static calculations. This is illustrated by the ‘approach—relax’ curves

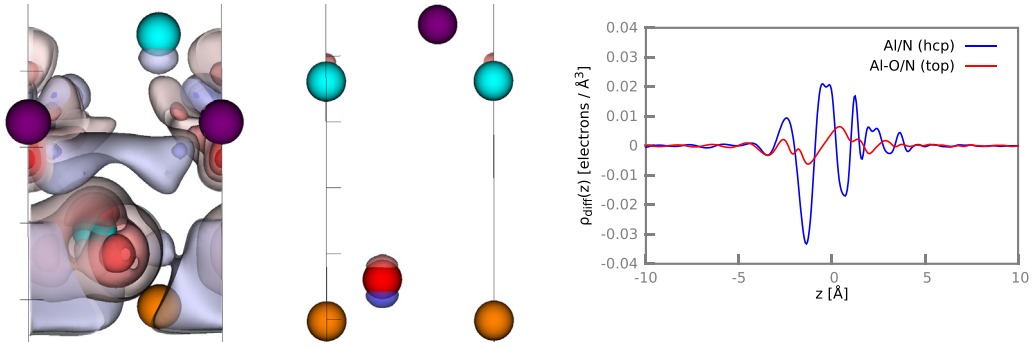

(a) (b) (c)

Figure 6. Charge-density differences ρ_{diff} (see equation (2)) at a (1 1 1) Al/TiN (N terminated) interface. ρ_{diff} was obtained from PBE calculations for the relaxed equilibrium configurations of (a) the Al/N (hcp) alignment and (b) the Al–O/N (top) alignment. In (a) and (b), isosurfaces of ρ_{diff} are plotted for values from -0.2 (blueish, deficit) to 0.3 (reddish, accumulation) electrons Å^{-3}. The solid black lines indicate the boundaries of the simulation cell. Color code: Al, orange; O, red; Ti, violet; N, cyan. In (c), the profiles of ρ_{diff} along the [1 1 1] direction of both interfaces shown in (a) and (b) are presented. Those profiles $\rho_{\text{diff}}(z)$ are calculated by two-dimensional integration. Negative values correspond to deficit of electrons. The x-axis gives the vertical distance z (along [1 1 1]) from the respective center of each interface.

which represent the interaction energies of the approaching slabs including atomic relaxations after each discrete step. Some of these curves exhibit rather large discontinuities which are either due to the Al slab expanding into the gap between the slabs, or due to material transfer between the slabs, particularly, from Al to TiN. Finally, the interaction energies, including atomic relaxations after each step, of the subsequent separation of the slab are given by the 'separation—relax' curves. These curves feature some kinks mainly because of the breaking apart of the Al/TiN compound into two separated slabs. When material transfer occurs, the separation curves start to deviate from the approach curves. The coloured curves represent configurations with relative strong interfacial interactions, while the grey curves show results for comparably weaker contacts.

Pristine Al slabs and TiN slabs interact strongly and exhibit adhesion energies of -1 to -2 eV for all alignments at the interface as well as for both TiN terminations [25]. Since these adhesion energies are always larger than the cost to remove Al layers from an Al slab, material transfer occurs for all configurations upon the separation of the two slabs. Depending on the equilibrium distance between two slabs typically one or two Al layers are transferred, because larger distances hinder the interaction between subinterface layers. Interaction-energy curves are presented in figure 7 for the limiting cases represented by the alignments hcp and top which results in the material transfer of two and one Al layer(s), respectively. For the Al/N (hcp) configuration structural snapshots along the separation are presented in figures 8(a)–(d).

The presence of oxygen at the interface between Al and TiN slabs reduces the adhesion energies between Al and TiN slabs significantly. In the case of N-terminated TiN the adhesion energy is diminished to just about -50 meV for all investigated alignments at the interface. This value is much smaller than the energy needed to remove material, here O and Al layers, from the oxygenated Al slab which is about -0.8 eV, see table 1. Thus, no material transfer should occur at these interfaces. Interaction-energy curves displayed in figure 7 for the approach and subsequent separation of oxygenated Al slabs and TiN slabs exhibit the predicted behaviour indicating no material transfer. Snapshots of the structures during the separation are shown in figures 8(e)–(h) for the Al–O/N (top) configuration. To check consistency, these calculations based on the PBE functional were repeated using LDA and optB86b. As expected the adhesion energies are increased for all configurations. Moreover, the ranges of the obtained values from about -0.1 eV to -0.25 eV and from about -0.22 eV to -0.31 eV for LDA and optB86b, respectively, for the different alignments are larger. The adhesion energies are, however, still significantly lower than the removal energies of about 1 eV (see table 1) for both functionals. Consequently, no material transfer occurs. Thus, the LDA and optB86b results are in agreement with PBE concerning material transfer. For non-oxygenated Al/TiN interfaces, results can be found in a previous publication [25]. There the occurrence of material transfer was demonstrated to be also independent of other computational settings, such as the size of the simulation cell as long as the surface structure is preserved. The obtained results are in line with the findings of other researchers that additional interfacial species like Mg, H, and Zn reduce the adhesion energies at Al/TiN interfaces [52, 58].

For Ti-terminated TiN slabs the adhesion energies at the Al/TiN interfaces are also reduced upon the introduction of oxygen at the interface. For different alignments at the interface the values of the adhesion energies range between -0.5 eV to -0.6 eV and -0.9 eV to -1.8 eV for the oxygenated and non-oxygenated [25] contact, respectively. The decrease is less pronounced than for the N-terminated case because of more favourable Ti–O interactions. Nevertheless, material transfer becomes again unfavourable because of the interfacial oxygen, since the adhesion energies become smaller than the Al–O removal energies of about -0.8 eV. The relevant information is summarized in table 2.

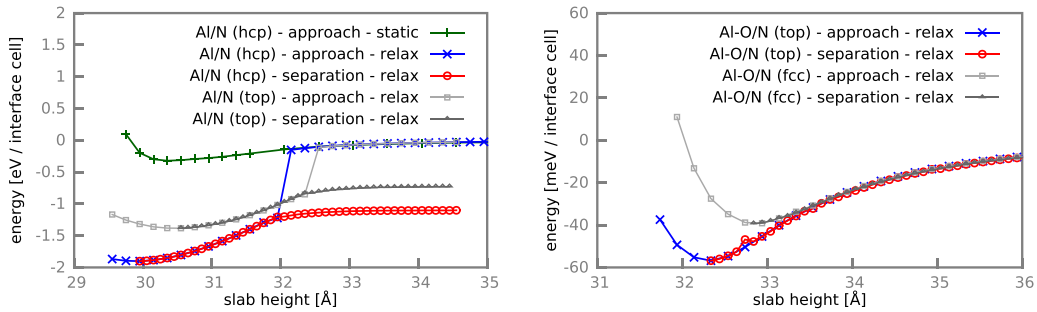

Figure 7. Calculated PBE interaction energies, see equation (1), for the approach and subsequent separation of (a) Al or (b) Al–O and TiN slabs for (1 1 1) N-terminated surface orientations. Subplot (a) is reproduced from [25]. The alignments follow the definitions in figure 2. Mind the different scales on the *y*-axes in subplots a and b. (a) (1 1 1) Al/TiN and (b) (1 1 1) Al–O/TiN.

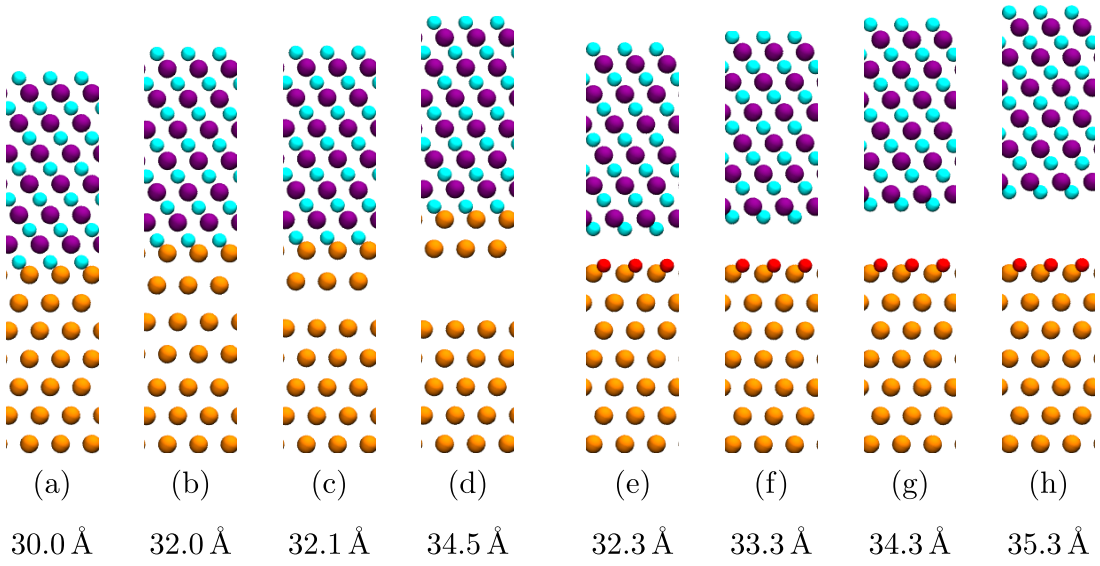

Figure 8. Separation of Al/N (hcp) (a)–(d) and Al–O/N (top) (e)–(h) aligned Al (1 1 1) and N-terminated TiN (1 1 1) slabs. Al, O, Ti, and N are coloured in orange, red, purple, and cyan, respectively. Subfigures (a) and (e) show the structures at the relaxed equilibrium distance. The steps are defined by the slab height. (a) 30.0 Å, (b) 32.0 Å, (c) 32.1 Å, (d) 34.5 Å, (e) 32.3 Å, (f) 33.3 Å, (g) 34.3 Å and (f) 35.3 Å.

3.4. Cu/C$_{dia}$ interfaces

In addition to the Al/TiN interfaces, Cu/C$_{dia}$ interfaces were investigated because of their high technological relevance and to test the used method for the simulation of material transfer on a different system. Analogous to the studies of Al/TiN, results on interfaces between the (1 1 1) surfaces of Cu/C$_{dia}$ are discussed in this section. Because of the qualitative similarity of the results and for the sake of space, only some major remarks and results are presented here.

In general, the diamond (1 1 1) surface exhibits a (2×1) reconstruction; however, in the case of hydrogen termination as well as at Cu/C$_{dia}$ interfaces no reconstructions are observed and (1×1) configurations are found [13, 61]. Thus, in this work only (1×1) structures are considered. At the diamond (1 1 1) surface two terminations are possible. Here, the single dangling bond configuration is assumed, because it is more stable for reasonable hydrogen chemical potentials than the triple dangling bond terminations [13, 62–65]. Particularly, the former configuration is more favourable at interfaces with copper [13].

The energy necessary to remove material from an (1 1 1) Cu slab is about 0.77 eV, which will be compared to the adhesion energies for several alignments at Cu/C$_{dia}$ interfaces in the following. Of the examined high symmetry contact configurations, which are defined in the same way as for the Al/TiN interfaces, the top and fcc alignments result in the strongest and weakest interfaces, respectively. The adhesion energy for the top configuration is about -1.05 eV, while for the fcc case it amounts to about -0.9 eV. Since these adhesion energies are larger than the cost to remove material from the Cu slab, material transfer is expected to occur for all configurations. Employing the method of approach and subsequent separation of the two slabs described above leads indeed to the material transfer of one layer of Cu towards the C$_{dia}$ slab for all tested contact scenarios, which are considered to be the limiting cases. Figures showing the corresponding interaction-energy curves are included in the supplemental material. These results support the DFT-based work of Guo *et al* [11] who predicted the occurrence of fracture at Cu/C$_{dia}$ interface between the first two metallic layers or the 2nd and the 3rd

Table 2. Equilibrium interface distances d_0 (Å), adhesion energies E_a (eV/interface cell), energy costs to remove layers from the Al slab E_r (eV/interface cell), and number of transferred Al layers (# TL) for various interface configurations between clean or oxygen covered Al and TiN surfaces. Al/Ti and Al/N denote the Ti- and N-terminated surfaces, respectively. All values were obtained using PBE. The results for the pristine interfaces are taken from [25].

	d_0	E_a	E_r	# TL
Al/N (hcp)	1.04	−1.90	0.80	2
Al/N (top)	1.87	−1.38	0.80	1
Al–O/N (fcc)	3.50	−0.04	0.80	0
Al–O/N (top)	3.01	−0.06	0.80	0
Al/Ti (hcp)	2.22	−1.78	0.80	2
Al/Ti (top)	2.67	−0.94	0.80	1
Al–O/Ti (hcp)	1.59	−0.54	0.80	0
Al–O/Ti (top)	1.61	−0.61	0.80	0

layers, because of a bond weakening resulting from the contact with the C_{dia} counterbody.

As for the Al/TiN interfaces, the effect of additional interfacial species was studied at the contact of Cu and C. Since the dangling bonds at diamond surfaces are often saturated by hydrogen atoms, this species was chosen for our investigation. At the C_{dia} (1 1 1) surface the H atoms prefer to sit at top sites in a distance of just 1.1 Å above each C atom forming a p(1 × 1) pattern. This is in good agreement with literature, e.g. in [13].

The adhesion energies for all studied contact configurations of the Cu/C_{dia} interfaces are extremely reduced to about −20 meV for hydrogen terminated C_{dia} surfaces in a similar fashion as for the oxygenated Al surfaces at the Al/TiN interfaces. Since these adhesion energies are much lower than the Cu removal energies of about 0.77 eV, no material transfer is expected. This predicted behaviour is verified by the method of approach and separation. Figures of the resulting interaction-energy curves are shown in the supplemental material.

The same results with respect to material transfer were obtained employing further XC functionals, namely LDA and vdW-optB86b. As expected using these functionals the adhesion as well as removal energies for all investigated interfaces are increased similar to the Al/TiN interfaces. For the clean surfaces LDA and vdW-optB86b yield very similar adhesion energies within about 10 meV for each configuration. These energies are about −1.21 eV and −1.34 eV for the fcc and top alignment, respectively. As for PBE, the adhesion energies are drastically reduced for interfaces involving hydrogenated C_{dia} surfaces. Using LDA the adhesion energies are between −0.11 eV for the fcc configuration and −0.13 eV for the top case, while for vdW-optB86b these energies range between about −0.15 eV and −0.16 eV for the corresponding alignments. The energies necessary to remove Cu layers from a Cu slab are also increased to 1.01 eV and 0.98 eV for LDA and vdW-optB86b, respectively. These results show that the choice of the investigated XC functionals does not affect the results for material transfer.

The findings presented above agree well with theoretical and experimental results presented in the introduction including the strong effect of interfacial hydrogen on the adhesion energy [13] and the possibility of a transfer of only one atomic layer of Cu [67]. Additionally, performing large-scale molecular dynamics (MD) simulations on the rubbing contact of hydrogenated diamond bodies and tungsten surfaces, Stoyanov *et al* [93] found that material transfer between C_{dia} and W mainly occurred at regions where the hydrogen had been depleted from the diamond surface because of the rubbing process. This observation is in qualitative agreement with our study finding material transfer only possible for non-hydrogenated diamond surfaces.

4. Conclusion and outlook

The adhesion energies at Al/TiN and Cu/C_{dia} interfaces are reduced significantly by the presence of a monolayer of oxygen and hydrogen at Al/TiN and Cu/C_{dia} interfaces, respectively. This reduction is investigated by analysing the densities of states and charge density differences at the aforementioned interfaces which reveal distinct bonding situations. Particularly, the possibility of material transfer at the interfaces is of interest. The occurrence of material transfer was studied by simulating the approach and subsequent separation of two slabs. For the clean surfaces material transfer of one or two atomic layers was found to be favourable for both investigated material combinations depending on the local interfacial configuration. The additional interfacial species O and H passivate the involved surfaces with respect to material transfer because of the strongly reduced adhesion energies for all investigated configurations. This agrees with the observation that metal-ceramic interfaces break in bulk areas or at the interface according to their interfacial adhesion [47, 48]. The results with respect to material transfer were not affected upon the use of different approximations for the XC functional, namely PBE, LDA, and optB86b.

The investigation of more complex interfacial species such as extended oxides instead of the studied monolayers promises to be very interesting in order to model many systems in a more realistic fashion. While, in principle, the method employed in this work can be applied to any pair of materials, in practice this can be computationally quite cumbersome. Large simulation cells, which translate into high computational demands, become necessary for complex materials or materials with an unfavourable bulk lattice mismatch because the translational symmetry has to be preserved and the lattice distortions should be as low as possible. On the other hand, larger cells allow to account for additional features such the minimization of lattice mismatches and the possibility to model dislocations or quasi-incommensurate contacts at interfaces. Furthermore, surface roughness can be treated to some extent by using a stepped surface or a regular arrangement of asperities.

Supplementary Data

See the Supplementary Data for more details on the computational settings, for orbitalresolved DOSs of the surface and interface layers of the strong Al(-O)/TiN interfaces, for DOSs

of the weaker Al(-O)/TiN interfaces as well as for figures showing interaction-energy curves for the Cu/Cdia interfaces.

Acknowledgments

The authors thank G Vorlaufer for fruitful discussions. GF is grateful for the financial support from the German Research Foundation (DFG) via SFB 986 M^3, project A4. GF, MW, POB, PM, and JR acknowledge the support by the Austrian Science Fund (FWF): F4109-N28 SFB ViCoM. Part of this work was funded by the Austrian COMET-Program (project K2 XTribology, No. 849109) via the Austrian Research Promotion Agency (FFG) and the Province of Niederösterreich, Vorarlberg, and Wien. Part of this work was supported by the European Cooperation in Science and Technology (COST; Action MP1303). This work was partially supported by the University of Modena and Reggio Emilia through the FAR project. The authors also appreciate the ample support of computer resources by the Vienna Scientific Cluster (VSC). Figures 1 and 2 were created employing VESTA [94], figure 6 utilizing VISIT [95], and figure 8 using VMD [96].

ORCID iDs

Gregor Feldbauer https://orcid.org/0000-0002-9327-0450
Michael Wolloch https://orcid.org/0000-0002-3419-5526

References

[1] Binnig G, Quate C and Gerber C 1986 *Phys. Rev. Lett.* **56** 930
[2] Kim S, Asay D and Dugger M 2007 *Nano Today* **2** 22
[3] Bhushan B 2008 *Phil. Trans. R. Soc.* A **366** 1499
[4] Bhushan B, Israelachvili J and Landman U 1995 *Nature* **374** 607
[5] Gnecco E, Bennewitz R and Meyer E 2002 *Phys. Rev. Lett.* **88** 215501
[6] Gotsmann B and Lantz M 2008 *Phys. Rev. Lett.* **101** 125501
[7] Bhaskaran H, Gotsmann B, Sebastian A, Drechsler U, Lantz M, Despont M, Jaroenapibal P, Carpick R, Chen Y and Sridharan K 2010 *Nat. Nanotechnol.* **5** 181
[8] Jacobs T and Carpick R 2013 *Nat. Nanotechnol.* **8** 108
[9] Kim H J, Yoo S S and Kim D E 2012 *Int. J. Precis. Eng. Manuf.* **13** 1709
[10] Howe J 1993 *Int. Mater. Rev.* **38** 233
[11] Guo H, Qi Y and Li X 2010 *J. Appl. Phys.* **107** 033722
[12] Johansson L 1995 *Surf. Sci. Rep.* **21** 177
[13] Wang X G and Smith J 2001 *Phys. Rev. Lett.* **87** 186103
[14] Rühle M, Heuer A, Evans A and Ashby M 1992 *Acta Metall. Mater.* **40** VII
[15] Kawarada H 1996 *Surf. Sci. Rep.* **26** 205
[16] Vargel C 2004 *Corrosion of Aluminium* (Amsterdam: Elsevier)
[17] Zhong W and Tománek D 1990 *Phys. Rev. Lett.* **64** 3054
[18] Dag S and Ciraci S 2004 *Phys. Rev.* B **70** 241401
[19] Garvey M, Furlong O, Weinert M and Tysoe W 2011 *J. Phys.: Condens. Matter* **23** 265003
[20] Zilibotti G and Righi M 2011 *Langmuir* **27** 6862
[21] Cahangirov S, Ataca C, Topsakal M, Sahin H and Ciraci S 2012 *Phys. Rev. Lett.* **108** 126103
[22] Kwon S, Ko J H, Jeon K J, Kim Y H and Park J 2012 *Nano Lett.* **12** 6043
[23] Bedolla P, Feldbauer G, Wolloch M, Gruber C, Eder S, Dörr N, Mohn P, Redinger J and Vernes A 2014 *J. Phys. Chem.* C **118** 21428
[24] Wolloch M, Feldbauer G, Mohn P, Redinger J and Vernes A 2014 *Phys. Rev.* B **90** 195418
[25] Feldbauer G, Wolloch M, Bedolla P, Mohn P, Redinger J and Vernes A 2015 *Phys. Rev.* B **91** 165413
[26] Wolloch M, Feldbauer G, Mohn P, Redinger J and Vernes A 2015 *Phys. Rev.* B **91** 195436
[27] Finnis M 1996 *J. Phys.: Condens. Matter* **8** 5811
[28] Lundqvist B *et al* 2001 *Surf. Sci.* **493** 253
[29] Sinnott S and Dickey E 2003 *Mater. Sci. Eng.* R **43** 1
[30] Thompson P and Robbins M 1989 *Phys. Rev. Lett.* **63** 766
[31] Robbins M and Müser M 2000 *Modern Tribology Handbook* vol 5 (Boca Raton, FL: CRC) pp 717–65
[32] Kenny S, Mulliah D, Sanz-Navarro C and Smith R 2005 *Phil. Trans. R. Soc.* A **363** 1949
[33] Schall J, Mikulski P, Chateauneuf G, Gao G and Harrison J 2007 *Superlubricity* (Amsterdam: Elsevier) pp 79–102
[34] Szlufarska I, Chandross M and Carpick R 2008 *J. Phys. D: Appl. Phys.* **41** 123001
[35] Vernes A, Eder S, Vorlaufer G and Betz G 2012 *Faraday Discuss.* **156** 173
[36] Eder S, Feldbauer G, Bianchi D, Cihak-Bayr U, Betz G and Vernes A 2015 *Phys. Rev. Lett.* **115** 025502
[37] Eder S, Cihak-Bayr U, Vernes A and Betz G 2015 *J. Phys. D: Appl. Phys.* **48** 465308
[38] Eder S, Bianchi D, Cihak-Bayr U and Gkagkas K 2017 *Comput. Phys. Commun.* **212** 100
[39] Eder S J, Cihak-Bayr U, Bianchi D, Feldbauer G and Betz G 2017 *ACS Appl. Mater. Interfaces* **9** 13713
[40] Ercolessi F and Adams J 1994 *Europhys. Lett.* **26** 583
[41] Jaramillo-Botero A, Naserifar S and Goddard W 2014 *J. Chem. Theory Comput.* **10** 1426
[42] Csányi G, Albaret T, Payne M and De Vita A 2004 *Phys. Rev. Lett.* **93** 175503
[43] Moras G, Ciacchi L, Elsässer C, Gumbsch P and De Vita A 2010 *Phys. Rev. Lett.* **105** 075502
[44] Kermode J, Ben-Bashat L, Atrash F, Cilliers J, Sherman D and De Vita A 2013 *Nat. Commun.* **4** 2441
[45] Avinun M *et al* 1998 *Thin Solid Films* **320** 67
[46] Chun J S, Desjardins P, Lavoie C, Shin C S, Cabral C, Petrov I and Greene J 2001 *J. Appl. Phys.* **89** 7841
[47] Howe J 1993 *Int. Mater. Rev.* **38** 257
[48] Ernst F 1995 *Mater. Sci. Eng.* R **14** 97
[49] Liu L, Wang S and Ye H 2004 *Acta Mater.* **52** 3681
[50] Song J and Srolovitz D 2006 *Acta Mater.* **54** 5305
[51] Zhang H, Liu L and Wang S 2007 *Comput. Mater. Sci.* **38** 800
[52] Zhang H and Wang S 2007 *J. Phys.: Condens. Matter* **19** 226003
[53] Yadav S, Ramprasad R, Misra A and Liu X Y 2012 *J. Appl. Phys.* **111** 083505
[54] Yadav S, Ramprasad R, Wang J, Misra A and Liu X Y 2014 *Modell. Simul. Mater. Sci. Eng.* **22** 035020
[55] Yadav S, Shao S, Wang J and Liu X Y 2015 *Sci. Rep.* **5** 17380
[56] Li N, Yadav S, Wang J, Liu X Y and Misra A 2015 *Sci. Rep.* **5** 18554
[57] Lin Z, Peng X, Fu T, Zhao Y, Feng C, Huang C and Wang Z 2017 *Physica* E **89** 15
[58] Liu L, Wang S and Ye H 2005 *J. Phys.: Condens. Matter* **17** 5335
[59] Jacobsen J, Hammer B, Jacobsen K W and Nørskov J 1995 *Phys. Rev.* B **52** 14954
[60] Jennison D and Bogicevic A 2000 *Surf. Sci.* **464** 108
[61] Schaich T, Braun J, Toennies J, Buck M and Wöll C 1997 *Surf. Sci.* **385** L958
[62] Scholze A, Schmidt W and Bechstedt F 1996 *Phys. Rev.* B **53** 13725
[63] Kern G, Hafner J and Kresse G 1996 *Surf. Sci.* **366** 445

[64] Kern G, Hafner J and Kresse G 1996 *Surf. Sci.* **366** 464
[65] Kern G, Hafner J and Kresse G 1997 *Surf. Sci.* **384** 94
[66] Pepper S 1982 *J. Vac. Sci. Technol.* **20** 643
[67] Zhu P and Fang F 2016 *Comput. Mater. Sci.* **118** 192
[68] Kresse G and Hafner J 1993 *Phys. Rev.* B **47** 558
[69] Kresse G and Hafner J 1994 *Phys. Rev.* B **49** 14251
[70] Kresse G and Furthmüller J 1996 *Phys. Rev.* B **54** 11169
[71] Kresse G and Furthmüller J 1996 *Comput. Mater. Sci.* **6** 15
[72] Blöchl P 1994 *Phys. Rev.* B **50** 17953
[73] Kresse G and Joubert D 1999 *Phys. Rev.* B **59** 1758
[74] Perdew J, Burke K and Ernzerhof M 1996 *Phys. Rev. Lett.* **77** 3865
[75] Perdew J and Zunger A 1981 *Phys. Rev.* B **23** 5048
[76] Klimeš J, Bowler D and Michaelides A 2009 *J. Phys.: Condens. Matter* **22** 022201
[77] Klimeš J, Bowler D and Michaelides A 2011 *Phys. Rev.* B **83** 195131
[78] Stampfl C and Van de Walle C 1999 *Phys. Rev.* B **59** 5521
[79] van de Walle A and Ceder G 1999 *Phys. Rev.* B **59** 14992
[80] Grabowski B, Hickel T and Neugebauer J 2007 *Phys. Rev.* B **76** 024309
[81] Csonka G I, Perdew J P, Ruzsinszky A, Philipsen P H T, Lebègue S, Paier J, Vydrov O A and Ángyán J G 2009 *Phys. Rev.* B **79** 155107
[82] Michaelides A and Scheffler M 2014 *Surface and Interface Science* ed K Wandelt (New York: Wiley) pp 13–72
[83] Graziano G, Klimeš J, Fernandez-Alonso F and Michaelides A 2012 *J. Phys.: Condens. Matter* **24** 424216
[84] Bedolla P, Feldbauer G, Wolloch M, Eder S, Dörr N, Mohn P, Redinger J and Vernes A 2014 *J. Phys. Chem.* C **118** 17608
[85] Antlanger M, Mayr-Schmölzer W, Pavelec J, Mittendorfer F, Redinger J, Varga P, Diebold U and Schmid M 2012 *Phys. Rev.* B **86** 035451
[86] Carrasco J, Liu W, Michaelides A and Tkatchenko A 2014 *J. Chem. Phys.* **140** 084704
[87] Matos J, Yildirim H and Kara A 2015 *J. Phys. Chem.* C **119** 1886
[88] Monkhorst H and Pack J 1976 *Phys. Rev.* B **13** 5188
[89] Methfessel M and Paxton A 1989 *Phys. Rev.* B **40** 3616
[90] Marlo M and Milman V 2000 *Phys. Rev.* B **62** 2899
[91] Wang C, Dai Y, Gao H, Ruan X, Wang J and Sun B 2010 *Solid State Commun.* **150** 1370
[92] Reguzzoni M, Fasolino A, Molinari E and Righi M C 2012 *Phys. Rev.* B **86** 245434
[93] Stoyanov P, Romero P, Merz R, Kopnarski M, Stricker M, Stemmer P, Dienwiebel M and Moseler M 2014 *Acta Mater.* **67** 395
[94] Momma K and Izumi F 2011 *J. Appl. Crystallogr.* **44** 1272
[95] Childs H *et al* 2012 *High Performance Visualization–Enabling Extreme-Scale Scientific Insight* (Boca Raton, FL: CRC Press) pp 357–72
[96] Humphrey W, Dalke A and Schulten K 1996 *J. Mol. Graphics* **14** 33